Increasing two-photon entangled dimensions by shaping input-beam profiles

Shilong Liu [1,2,*] Yingwen Zhang [3] Chen Yang,[1,2] Shikai Liu,[1,2] Zheng Ge,[1,2] Yinhai Li,[1,2] Yan Li,[1,2]
Zhiyuan Zhou,[1,†] Guangcan Guo,[1,2] and Baosen Shi[1,2,‡]

[1]*Key Laboratory of Quantum Information, University of Science and Technology of China, Hefei, Anhui 230026, China*

[2]*Synergetic Innovation Center of Quantum Information & Quantum Physics, University of Science and Technology of China,*
Hefei, Anhui 230026, China

[3]*National Research Council of Canada, 100 Sussex Drive, Ottawa, Ontario, Canada K1A0R6*

Photon pairs entangled in high-dimensional orbital angular momentum (OAM) degrees of freedom (DOF) have been widely regarded as a possible source for improving the capacity of quantum information processing. The generation of a high-dimensional maximally entangled state in the OAM DOF is therefore much desired. In this work, we demonstrate a simple method to generate a broader and flatter OAM spectrum, i.e., a larger spiral bandwidth (SB), of entangled photon pairs generated through spontaneous parametric down-conversion by modifying the pump beam profile. By investigating both experimentally and theoretically, we find that an exponential pump profile that is roughly the inverse of the mode profiles of the single-mode fibers used for OAM detection will provide a much larger SB compared to a Gaussian-shaped pump.

I. INTRODUCTION

The two-photon high-dimensional entangled state (HD-ES), $\sum_{j=0}^{d-1} c_j |j\rangle_A |j\rangle_B$, has been widely regarded as useful in increasing the capacity for quantum information processing. From the fundamental physics standpoint, such states imply a larger violation of local-realism theories and a lower fidelity bound in quantum state cloning [1–3]. Also, great attention has been given to their practical applications [3,4], for example, enhancing security robustness against eavesdrop in quantum cryptography [5,6], increasing dimensions of the Bell state in dense coding, entanglement swapping, or teleportation [7–9], multiplexing a heralded single-photon source [10,11], and improving the quality of imaging or quantum sensors [12–14].

In photonic systems, one can construct an HD-ES in many of the photon's degrees of freedom (DOF) [15,16], for example, in orbital angular momentum (OAM) [17–23], paths [24–26], frequency [27], photon number [28], and temporal modes [29,30]. HD-ESs in OAM have been gaining more attention due to their easy scalability in dimension. One typical process is to create 100×100–dimensional entanglement via employing both the OAM and the radial DOF of entangled photon pairs [31].

The most common method for generating OAM entangled photon pairs is via the process of spontaneous parametric down-conversion (SPDC) [17]. According to OAM conservation, the sum of OAM from the signal and idler photons must equal that of the pump photon, i.e., $\ell_p = \ell_s + \ell_i$. When $\ell_p = 0$, the output two-photon state of SPDC can be Schmidt decomposed into $\sum_{-\infty}^{\infty} C_{\ell_s,\ell_i} |-\ell\rangle_s |\ell\rangle_i$. Here, C_{ℓ_s,ℓ_i} is the probability amplitude ($\sum |C_{\ell_s,\ell_i}|^2 = 1$) of finding a signal photon with OAM $-\ell$ and an idler photon with OAM ℓ in coincidence. The width of the OAM spectrum is often known as the spiral bandwidth (SB) [32]. The Schmidt number $K = 1/\sum C_{\ell_s,\ell_i}^4$ is also often defined to evaluate the entanglement dimensions [33–35]; a larger value of K depicts a larger dimension of entanglement. For a maximally entangled state (MES) of $|C_{\ell_s,\ell_i}| = 1\sqrt{d}$, the Schmidt number is d. Entangled photons with a larger Schmidt number could be beneficial in implementing higher-dimensional quantum protocols like cryptography, computation, imaging, and metrology.

For SPDC, the coincidence amplitudes C_{ℓ_s,ℓ_i} can be calculated via the overlap integral between the input pump mode and both the signal and the idler modes in the Laguerre-Gaussian (LG) basis [34,36]. Previous works have shown several ways to increase the SB of OAM entanglement. First, one can adjust the beam waist ratio between the pump and the measured LG modes $\gamma = w_p/w_{s(i)}$ [32–34]; the SB increases with increasing γ. Second, one can change the down-conversion angle by adjusting the SPDC phase matching [35,37,38]; the SB changes based on the down-conversion angle between the SPDC photons. Finally, one can engineer a crystal with spatially varying phase matching [39–41]; there has been little experimental progress in this avenue due to the complex fabrication technology. Also, some works attempt to prepare HD-MESs through some complex engineering of the pump beam profile [23,42–46]. In recent work [44,45], a three-dimensional maximally entangled state $1/\sqrt{3}(|-1\rangle|-1\rangle + |0\rangle|0\rangle + |1\rangle|1\rangle)$ has been generated by shaping the pump into a superposition of several LG modes. However, the generation of higher-dimensional MESs remains difficult due to the crosstalk between OAM modes.

Here, we propose an ingenious method to increase the SB via some simple shaping of the pump beam profile. We show both theoretically and experimentally that an

*lslong@mail.ustc.edu.cn
†zyzhouphy@ustc.edu.cn
‡drshi@ustc.edu.cn

exponential pump will significantly flatten the OAM spectrum and extend the SB. The optimal exponential pump is when the combined profile of both single-mode optical fibers (SMFs) and pump beam profile is a constant, where the optimal pump is roughly the inverse of mode profile from the SMFs. We then perform high-dimensional quantum state tomography in three- and five-dimensional subspaces using the optimized exponential pump; the corresponding fidelities are 90.74% and 81.46% for three- and five- dimensional MESs, respectively. Traditionally, when the input pump beam profile is a Gaussian function, the distribution of the coincidence amplitude with OAM is strongly mode dependent [34,36]. Therefore, mode postselection has to be performed in order to generate an HD-MES. Our method demonstrates a simple way to broaden and flatten the SB, which could allow future quantum protocols using the OAM DOF to access higher-dimensional MESs without requiring mode filtering.

II. RESULTS

A. Optimizing the input beam profile to increase the entangled dimension

SPDC photons entangled in arbitrary superpositions of OAM are often described in terms of the LG modes. In our analysis, we are only interested in the OAM DOF and set the radial momenta to be 0. In the thin crystal limit, the phase-matching function of the SPDC process can be approximated to unity and the coincidence amplitudes C_{ℓ_s, ℓ_i} can be calculated from the overlap integral [34,47,48]

$$C_{\ell_s, \ell_i} = \int \Phi(\boldsymbol{x}) [\mathrm{LG}_{\ell_s}(\boldsymbol{x})]^* [\mathrm{LG}_{\ell_i}(\boldsymbol{x})]^* \mathrm{G}^2(\boldsymbol{x}) d^2 x, \quad (1)$$

where $\Phi(\boldsymbol{x})$ is the mode function of the pump and $\mathrm{G}(\boldsymbol{x})$ is the Gaussian mode of the SMF used for detection. $\mathrm{LG}_\ell(\boldsymbol{x})$ is the LG mode [49]. When the pump profile is a Gaussian and the LG mode sizes of the signal and idler beams are chosen to be equal, $w_s = w_i \equiv w_{si}$, the coincidence probability can be evaluated as [34,47,48]

$$C_{-\ell, \ell} \propto \left(\frac{2\gamma^2}{2\gamma^2 + 2\eta^2 + 1} \right)^{|\ell|}. \quad (2)$$

Here $\gamma = w_p / w_{si}$ is the beam waist ratio between that of the pump and the LG modes of the signal and idler photons measured on the nonlinear crystal plane. $\eta = w_p / w_f$ is the beam waist ratio between the pump beam and the mode size of the SMFs. Based on Eq. (2), the OAM spectrum always peaks at $\ell = 0$ and rapidly decreases with increasing ℓ.

Looking at Eq. (1), we see that if the combined profile (CP) of $\Phi(\boldsymbol{x})$ and $\mathrm{G}^2(\boldsymbol{x})$ is a constant, the overlap integral should be a constant with respect to ℓ resulting in an HD-MES [48]. We classically simulated this using Klyshko's advanced-wave representation [50]. It was found that the SB can be expanded significantly when this CP is flat. We look at a more general situation that uses an adjustable exponentially shaped pump beam whose beam profile is given by

$$\Phi(r) = \exp\left(\frac{ar^2}{w_p^2} \right) H(-r + w_p). \quad (3)$$

Here a is a parameter that determines the width and curvature of the exponential function and $H(x)$ is the heaviside step
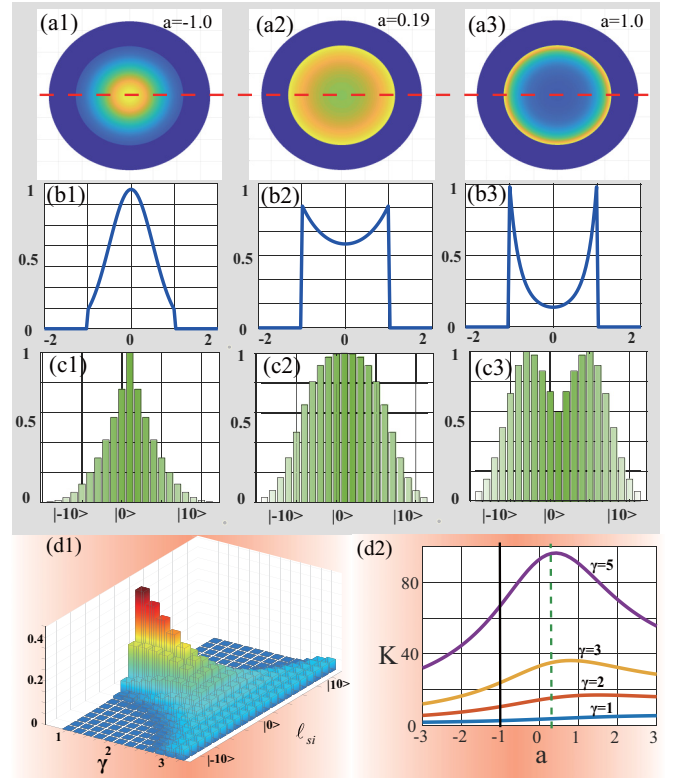

FIG. 1. Theoretical results in the OAM spectrum under various pump profiles. (a1–a3) Intensity pump beam profiles with $a = -1$, $a = 0.19$, and $a = 1.0$. (b1–b3) Corresponding cross-section profile of the pump [along the red line in (a1)–(a3)]. (c1–c3) Theoretically predicted OAM spectrum based on Eq. (4), where $\gamma = w_p / w_{si}$ is equal to 2.0 and $\eta = w_p / w_f$ is equal to 0.31. (d1) OAM spectrum along different γ values, where the pump beam profile is set to $a = 0.19 = 2\eta^2$. (d2) Schmidt number versus beam profile parameter of a running from -3 to 3 for various γ values, with OAM ranging from -50 to 50 in the calculations. The left solid and right dashed vertical lines in (d2) represent the pump beam profile of a Gaussian $a = -1$ and an exponential with $a = 2\eta^2 = 0.19$, respectively.

function, which limits the width of the beam to the same. After evaluating the overlap integral in Eq. (1), $C_{-\ell, \ell}$ is determined to be

$$C_{-\ell, \ell} \propto \left(\frac{2\gamma^2}{2\gamma^2 + 2\eta^2 - a} \right)^{|\ell|}$$
$$\times \left[1 - \frac{1}{|\ell|!} \Gamma(1 + |\ell|, 2\gamma^2 + 2\eta^2 - a) \right], \quad (4)$$

with $\Gamma(n, z)$ $(= \int_z^\infty t^{n-1} e^{-t} dt)$ being the incomplete gamma function.

Equation (4) is similar to Eq. (2), despite the extra gamma function. Some interesting behavior can be observed when a is varied.

i. When $a < 2\eta^2$, the CP of the pump and the SMFs is still a Gaussian. The OAM spectrum is essentially the same as that in Eq. (2) (with some small deviations coming from the incomplete gamma function at larger ℓ), where it peaks at $|\ell| = 0$ and decreases rapidly with larger $|\ell|$ values [Fig. 1(a1)]. The SB broadens as a approaches $2\eta^2$.
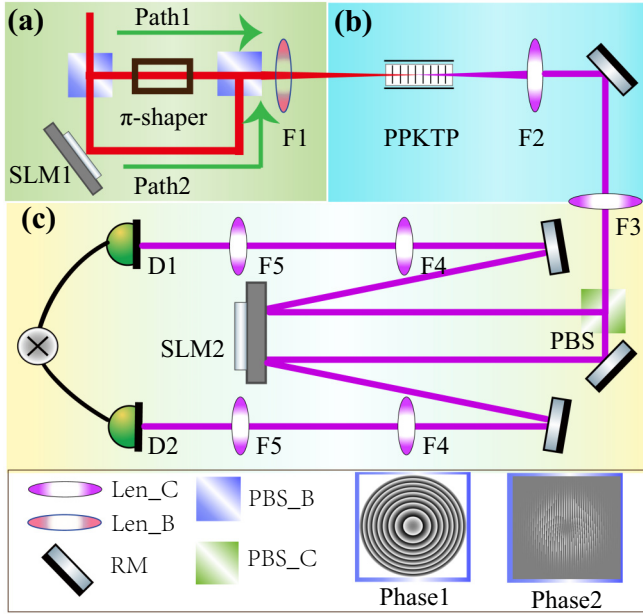
FIG. 2. Experimental setup for pump shaping, generation, and detection of OAM entangled photons. The pump beam is first shaped either by SLM1 (i.e., phase 1 for $a = 0$) or by the π shaper into the desired beam shape. The beam then pumps a 10-mm-long PPKTP crystal (type II; 775 to 1550 nm) to generate OAM entangled photon pairs via SPDC. Through the use of SLM2 (i.e., phase 2 for $\ell = 1$) and single-mode fibers, projective measurements of the photons' OAM can be performed.

ii. When $a = 2\eta^2$, the CP will have a flattop. The first term in Eq. (4) becomes a constant resulting in a flat OAM spectrum, however, the incomplete gamma function will suppress $|C_{-\ell,\ell}|^2$ for larger $|\ell|$ values [Fig. 1(a2)]. To further broaden the OAM spectrum, one can increase γ as shown in Fig. 1(d1).

iii. When $a > 2\eta^2$, the CP is an exponential. The denominator in the first term of Eq. (4) is now smaller than its numerator, so the term will increase with increasing $|\ell|$. $|C_{-\ell,\ell}|^2$ is still suppressed by the incomplete gamma function at larger $|\ell|$ values. This results in an OAM spectrum that peaks at some nonzero $|\ell|$ value [Fig. 1(a3)].

In Fig. 1(d2), it can be seen that for larger γ values, the Schmidt number reaches a maximum when $a \approx 2\eta^2$. However, when γ is small, the maximum Schmidt number occurs at $a > 2\eta^2$. This is the result of a larger contribution from the incomplete gamma function when γ is small, therefore suppressing $C_{-\ell,\ell}$ at smaller ℓ values.

B. Beam-shaping technology for two-photon high-dimensional entanglements

To verify the theoretical prediction in Eq. (4), we measured two-photon OAM correlations using different input beam profiles (parameter a). The corresponding experimental setup is shown in Fig. 2, which includes three parts: pump beam shaping [Fig. 2(a)], state generations [Fig. 2(b)], and projection measurements [Fig. 2(c)]. First, the pump beam was shaped using either an SLM (path 2) or a π shaper (path 1) from a Gaussian into the desired beam shape (details in
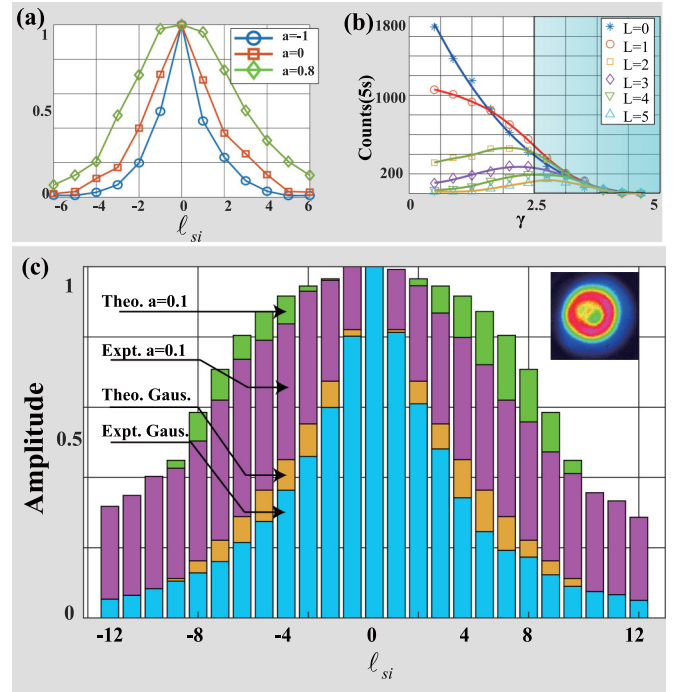

FIG. 3. Normalized OAM spectrum in SPDC. (a) OAM spectrum for various pump profiles. Here, $\gamma = 1.25$ and $\eta = 0.31$. (b) Coincidences for various ℓ values as a function of γ when the pump profile has $a = 0.10$. (c) OAM spectrum measured from $\ell = -12$ to $l = 12$ for $\gamma = 2.4$. The green (fourth, innermost layer) and red (third layer) OAM spectra are normalized theoretical and experimental results for $a = 0.10$, respectively; the corresponding Gaussians $a = -1$ are shown by orange (second layer) and blue (first, outermost layer) bars. Inset in (c): Optimized pump beam profile, where we can estimate the parameter $a = 0.10$ by fitting its intensity. The nonnormalized versions of (a) and (c) can be found in Appendix A.

Appendix A). Then a 10-mm-long nonlinear crystal (PPKTP) was placed at the beam waist to perform the SPDC process. The spatial photons on the nonlinear crystal plane were imaged to the surface of another SLM for mode demodulation and then for coincidence measurements via a superconducting nanowire single-photon detector. In our setup, the beam width ratio η is 0.31. It should be noted that though an SLM has more versatility in the beam shaping it can perform, it cannot support high pump intensities and has lower conversion efficiencies compared to a commercial π shaper. The SLM is therefore used in confirming the shape of the SB for various a parameters; in situations where a high pump power (350 mW) is required to increase the SPDC photon production rate and reduce the data acquisition time without needing to change the beam shape, the π shaper is used.

C. Two-photon OAM spectrum under different beam profiles

Figure 3(a) shows the OAM spectrum generated with different pump beam profiles ($a = -1$, 0, and 0.8) reported in Appendix A, where the beam width ratio γ is 1.25. It can be seen that the OAM spectrum broadens as a increases, just as theoretically predicted from Eq. (4). Also, note that since

γ is small, the optimized beam profile a [the largest SB (or K)] is actually larger than $2\eta^2$ as shown in Fig. 1(d2). The theoretical OAM spectra for these three cases are given in Appendix A.

In addition to the beam profile parameter a, the beam width ratio γ is another important parameter that affects the entangled dimension. In Fig. 3(b), we show the measured coincidence rate for various ℓ values as a function of γ, where $a = 0.10$. One can see that for larger values of γ [blue area in Fig. 3(b); $\gamma \geqslant 2.5$], the differences in coincidence rate for the various ℓ values are relatively small, which indicates a broader SB. This is in agreement with our theoretical results shown in Fig. 1(d1).

In Fig. 3(c) we show the theoretical and experimental OAM spectra from $\ell = -12$ to $\ell = 12$ for $\gamma = 2.4$. A significantly broader OAM spectrum can be observed compared to a Gaussian pump ($a = -1$) with the same γ. The experimental azimuthal Schmidt number K is determined to be 21.9, which is in good agreement with the theoretical prediction of 20.7; for a Gaussian pump K is 15. For quantifying the crosstalk between two neighboring OAM values, we measured the crosstalk visibility $(1 - \sum_{i,j=i\pm1} C_{i,j}^2 / \sum_{i=-12}^{12} C_{ii}^2)$ and obtained a value of 93.91%.

D. Quantum state tomography of high-dimensional entanglement

From Fig. 3(c), one can see that the HD-MES is prepared in at least a five-dimensional subspace. We reconstructed the density matrices for the cases of dimensions $d = 3$ [Figs. 4(a) and 4(b)] and $d = 5$ [Figs. 4(c) and 4(d)] through high-dimensional quantum state tomography [45,51,52] (also see Appendix B). The measured fidelity, $F = [\text{Tr}\sqrt{\sqrt{\rho}\rho_{\text{exp}}\sqrt{\rho}}]^2$, was 0.9071 ± 0.005 for $d = 3$ and 0.8146 ± 0.0014 for $d = 5$, with the uncertainty obtained through statistical simulations assuming that the coincidence events follow a Poissonian distribution. The fidelity for both $d = 3$ and $d = 5$ entangled states exceeded the dimensional threshold of $(d - 1)/d$, signifying that the density matrix cannot be decomposed into an ensemble of pure states with a low Schmidt number [53–55]. The fact that the fidelity of the $d = 5$ MES is less than that of the $d = 3$ is not surprising, as Fig. 3(c) shows that the OAM spectrum is fairly flat at $d = 3$ ($\ell = -1, 0, 1$) but less so at $d = 5$ ($\ell = -2, -1, 0, 1, 2$). One can improve the fidelity for higher dimensions by using a slightly higher beam waist ratio γ. From the density matrix we can also calculate the linear entropy, $S_{\text{ent}} = 1 - \text{Tr}(\rho_{\text{exp}}^2)$, giving $S_{\text{ent}} = 0.1043 \pm 0.009$ and 0.2851 ± 0.0093 for the $d = 3$ and $d = 5$ cases, respectively; the linear entropy determined using the theoretical OAM spectrum is 4×10^{-4} for $d = 3$ and 12×10^{-4} for $d = 5$ (for a pure state the linear entropy is 0). Furthermore, the CGLMP Bell inequality [2] was determined to be 2.85 ± 0.03 and 2.40 ± 0.01 for the $d = 3$ and $d = 5$ entangled states, respectively. As a comparison, the theoretical upper bound for the CGLMP Bell inequality is 2.87 and 2.91 for the $d = 3$ and $d = 5$ entangled states, respectively [2]. The lower value for the $d = 5$ case is mainly attributed to imperfect mode overlap between the SPDC photons and the measurement SLM. These values are listed in the table in Fig. 4 for clarity.

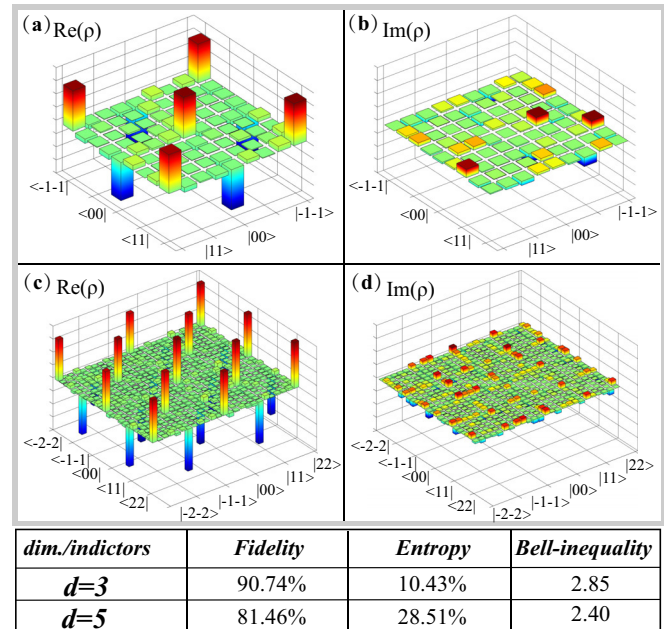| dim./indictors	Fidelity	Entropy	Bell-inequality
d=3	90.74%	10.43%	2.85
d=5	81.46%	28.51%	2.40

FIG. 4. Reconstructed density matrices of three- and five-dimensional OAM MESs from the experimental OAM spectrum in Fig. 3(c). (a), (b) Real and imaginary parts of the density matrix for $d = 3$. (c), (d) Real and imaginary parts of the density matrix for $d = 5$. The table at the bottom displays the corresponding fidelity, entropy, and CGLMP Bell inequality for the two density matrices. Data acquisition times for each reading are 50 and 300 s for the three- and five-dimensional cases, respectively.

III. DISCUSSION

In this work, a simple technique for shaping pump beam profiles to increase the two-photon OAM entanglement dimensions in SPDC processes is demonstrated. Theoretically and experimentally, we found that the coincidence amplitude will become mostly mode independent when the pump profile is an exponential that roughly cancels the Gaussian profile of the SMFs used for photon detection. Compared to the more commonly used method of increasing γ to expand the OAM entanglement dimensions, optimizing the beam profile in SPDC offers two advantages. First, by optimizing the beam profile one does not suffer as much loss to the coincidence count rate compared to increasing γ, which can lead to a significant reduction in the coincidence count rate due to a decrease in the coupling efficiency to the SMFs. Second, by shaping the pump into an inverse Gaussian, one can always achieve an OAM spectrum that is flat for at least several OAM modes even in cases where γ is small (≈ 2 or less); this allows one to generate an HD-MES in situations not possible previously. This adds a way to expand the SPDC OAM spectrum and can be used concurrently with previously suggested techniques such as increasing γ and adjusting the down-conversion angle between the signal and the idler photons. The ability to generate such HD-MESs without mode postselection will be of great importance in quantum communication, quantum sensing, and, also, fundamental physics research.

APPENDIX A: SHAPING THE BEAM PROFILE VIA DIFFRACTIVE OPTICS

When a monochrome electronic field $U(x_1, y_1)$ passes a lossless phase element, the mapping of the output field can be expressed in terms of the Fresnel integral. Usually, a lens (f) is used to focus the beam waist located after the phase element. The beam-shaping problem can be seen as a Fourier transform [56,57],

$$U(x, y) = \frac{1}{i\lambda f} \exp(ikf + x^2 + y^2)$$
$$\times \iint U(x_1, y_1) \exp(i\beta\phi(x_1, y_1))$$
$$\times \exp\left(-i\frac{2\pi}{\lambda f}(xx_1 + yy_1)\right)dx_1 dy_1, \quad \text{(A1)}$$

where $k = 2\pi/\lambda$, and $U(x_1, y_1)$ and $U(x, y)$ are the magnitudes of the input and output fields, respectively. The beam-shaping problem is to determine what the phase function $\beta\phi(x_1, y_1)$ is. Here, $\beta(= 2\pi w_0 w_1/\lambda f)$ is a system parameter connecting the input beam width w_0 with the output beam width w_1. In principle, any arbitrary field can be shaped approximately through a suitable phase function. A suitably large β can generate a good approximate output field [56].

Based on the diffraction theory of lossless beam shaping [56], three steps are needed to determine the phase factor ϕ. For a radially symmetric problem, first, we need to evaluate the constant A given by

$$A = \frac{\int_{-\infty}^{+\infty} I(s)ds}{\int_{-\infty}^{+\infty} Q(s)ds}, \quad \text{(A2)}$$

where the $I(s)$ and $Q(s)$ are the intensities of the input and output beams. Then the phase factor ϕ can be determined by solving two ordinary differential equations [56],

$$AQ(\alpha)\frac{d\alpha}{d\xi} = I(\xi),$$
$$\frac{d\phi}{d\xi} = \alpha(\xi), \quad \text{(A3)}$$

where $\alpha(\xi)$ is a medium function. For some certain special patterns, the ordinary differential equations can be solved analytically; for example, for the output as a flattop beam [$Q(s) = 1 * H(-s + 1)$], the phase can be given,

$$\phi(\xi) = -\frac{2}{\pi}\left(\xi\frac{\sqrt{\pi}}{2}\exp(\xi) + \frac{1}{2}\exp(-\xi^2) - \frac{1}{2}\right). \quad \text{(A4)}$$

In most situations, one needs to solve for ϕ numerically, which is the case when the output beam profile is an exponential
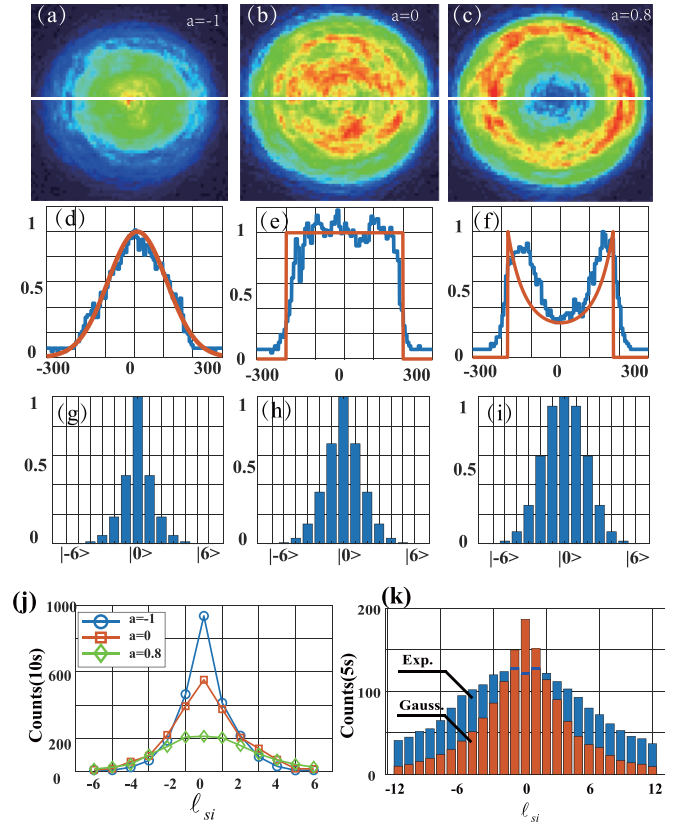

FIG. 5. Intensity patterns of the pump beam profiles and the corresponding OAM spectrum. (a)–(c) Pump beams generated in our system with $a = -1$, 0, and 0.8, respectively. (d)–(f) Corresponding cross-section intensity profile [along the white line through (a)–(c)]. Wavy blue lines show the measured distributions, and smooth red lines the theoretical distributions. (g)–(i) Corresponding theoretical OAM spectrum with $\gamma = 1.25$. (j), (k) Experimental OAM spectra corresponding to Figs. 3(a) and 3(c), respectively. In Fig. 3(c), the outermost, red distribution is the situation of the Gaussian pump, and the innermost, blue bars show the situation of the optimized exponential pump.

function, $Q(s) = \exp(as^2)$, as in this paper. Experimentally, we can realize the beam shaping by loading the phase $\beta\phi$ onto an SLM. In our setup (Fig. 2 in the text), the Fourier lens (F1) has a focal length of 75 mm, the input beam waist is 3000 μm, and the beam width of the output beam is set to 200 μm on the Fourier plane. Therefore, one can determine $\beta = 64.4$. Figures 5(a)–5(c) show some intensity patterns of the input beams with the exponential function. The corresponding cross-section distributions are shown in Figs. 5(d)–5(f). Under these beams as a pump, we get the theoretical OAM spectrum, which is shown in Figs. 5(g)–5(i). Figure 5(j) shows the corresponding experimental results, where three lines represent three situations of pumps in $a = -1$, $a = 0$, and $a = 0.8$, respectively. Figure 5(k) is the measured OAM spectrum when the situations of the pumps are the optimized and Gaussian beams, respectively, where we use the π shaper to generate the optimized pump beam.

The SLM used could not support a very high input power and has a low conversion efficiency (about 30% at first

order). Therefore, we employed a commercial π shaper to perform beam shaping when a high pump power was required to increase SPDC photon production and reduce the data acquisition time. In this regime, a π shaper and a Fourier lens ($f = 1000$ mm) are used to shape the beam profile. A π shaper is used to transform a Gaussian into an Airy disk via the Fourier-Bessel transformation [58,59],

$$I_f(\rho) = I_{f0}[J_0(2\pi\rho)/2\pi\rho]^2, \tag{A5}$$

where $J_0(2\pi\rho)$ is the zeroth-order Bessel function of the first kind and I_{f0} is the normalization factor. Such a beam can be transformed into a flattop beam in the Fourier plane by using a Fourier lens. The change in the shape of $I(\rho)$ as it propagates can be determined by the Rayleigh-Sommerfeld diffraction integral [60]. An exponential-like beam shape would be created at a location slightly away from the Fourier plane. Experimentally, we could move the nonlinear crystal along the beam axis slightly to the location with the desired beam shape.

APPENDIX B: DETAILS OF HIGH-DIMENSIONAL QUANTUM ENTANGLED STATE TOMOGRAPHY

For a high-dimensional entangled state (MES), the theoretical density matrices can be given as

$$\rho = |\psi\rangle_{\text{MES}} \otimes \langle\psi|_{\text{MES}} . \tag{B1}$$

Using this definition, we can calculate the theoretical density matrix ρ of the MES [52].

Experimentally, with the help of projection measurement, one can reconstruct the density matrix of a high-dimensional MES. For an HD-MES defined in d-dimensional space, the corresponding reconstructed density matrices can be written as [51]

$$\rho_{\text{exp}} = N \sum_{u,v,j,k=1}^{d^2} \left(A_{uv}^{jk}\right)^{-1} n_{uv} \lambda_j \otimes \lambda_k, \tag{B2}$$

where N is the normalized coefficient; $A_{uv}^{jk}(= \langle\Psi_{uv}| \lambda_j \otimes \lambda_k |\Psi_{uv}\rangle)$ is the constant matrix associated with the fundamental matrix $\lambda_{j,k}$ and measurement basis $|\Psi_{uv}\rangle$, in which $\lambda_{j,k}$ can be generated by SU(d) algebra; $|\Psi_{u,v}\rangle = |\Psi_u\rangle_A |\Psi_v\rangle_B^\dagger$ represents the measurement basis in the signal (A) and idler photons (B); $(A_{uv}^{jk})^{-1}$ are the corresponding inverted matrices; and $n_{uv} = N\text{tr}(\Pi_{A,B}\rho_{\text{exp}})$ represents the coincidence counts measured by electronic systems [52]. In order to experimen-

tally reconstruct the density matrix of HD-MES, three steps should be performed as follows.

1. Ensure the details of the projection measurement basis

The first step is to ensure the details of the projection measurement basis. The constant matrix A_{uv}^{jk} is associated with the measurement basis $|\Psi_{uv}\rangle$. One can set the measurement basis to a complete group of mutually unbiased bases (MUBs) $\{|\Psi_m^j\rangle\}$, which can be generated using the Weyl group, Hadamard matrix, or Fourier-Gauss transform method [61]. Here, we used the discrete Fourier-Gauss transform to product MUBs in prime dimensional space [62],

$$\left\{\left|\Psi_m^j\right\rangle\right\} = \left\{\frac{1}{\sqrt{d}} \sum_{n=0}^{d-1} \omega_d^{(jn^2+nm)} |n\rangle\right\}, \tag{B3}$$

where j ($j = 0 \ldots d-1$) indexes the group of MUBs, m ($m = 0 \ldots d-1$) indexes the superposed OAM states for each set of MUBs, and $|\langle\Psi_m^j|\Psi_{m'}^{j'}\rangle|^2 = 1/d(1 - \delta_{jj'})$ for the MUBs. In actuality, j runs from 0 to d, with the last set of MUBs being the OAM eigenstates.

2. Obtain a series of coincidence photon counts

After setting the details of the MUBs, one next performs projection measurement to get coincidence photon counts n_{uv} under these MUBs, called OAM superposition states. Experimentally, we employ amplitude-encoding technology to generate high-fidelity OAM MUBs [63,64].

3. Calculate the experimental density matrix

Finally, based on Eq. (B2), we calculate the density matrix ρ_{exp}, and thus get the fidelity and entropy. It should be noted that the reconstructed density matrix may not be a 'physical' density matrix, i.e., it has the property of positive semidefiniteness [65]. To overcome this disadvantage, the maximum likelihood estimation method is used during the process of reconstructions. We build the likelihood function,

$$L(t_1, t_2, \ldots, t_{d^4}) = \sum_{j=1}^{d^4} \frac{[N(\langle\Psi_j| \rho_{\text{exp}} |\Psi\rangle_j - n_j]^2}{2N(\langle\Psi_j| \rho_{\text{exp}} |\Psi\rangle_j}, \tag{B4}$$

where ρ_{exp} should be preliminary defined as a physical density matrix [65].

[1] A. C. Dada, J. Leach, G. S. Buller, M. J. Padgett, and E. Andersson, Nat. Phys. **7**, 677 (2011).

[2] D. Collins, N. Gisin, N. Linden, S. Massar, and S. Popescu, Phys. Rev. Lett. **88**, 040404 (2002).

[3] M. Erhard, R. Fickler, M. Krenn, and A. Zeilinger, Light: Sci. Appl. **7**, 17146 (2018).

[4] A. M. Yao and M. J. Padgett, Adv. Opt. Photon. **3**, 161 (2011).

[5] M. Mirhosseini, O. S. Magaña-Loaiza, M. N. OSullivan, B. Rodenburg, M. Malik, M. P. Lavery, M. J. Padgett, D. J. Gauthier, and R. W. Boyd, New J. Phys. **17**, 033033 (2015).

[6] N. J. Cerf, M. Bourennane, A. Karlsson, and N. Gisin, Phys. Rev. Lett. **88**, 127902 (2002).

[7] F. Wang, M. Erhard, A. Babazadeh, M. Malik, M. Krenn, and A. Zeilinger, Optica **4**, 1462 (2017).

[8] X.-M. Hu, C. Zhang, B.-H. Liu, Y.-F. Huang, C.-F. Li, and G.-C. Guo, arXiv:1904.12249.

[9] Y.-H. Luo, H.-S. Zhong, M. Erhard, X.-L. Wang, L.-C. Peng, M. Krenn, X. Jiang, L. Li, N.-L. Liu, C.-Y. Lu, A. Zeilinger, and J.-W. Pan, Phys. Rev. Lett. **123**, 070505 (2019).

[10] M. Grimau Puigibert, G. H. Aguilar, Q. Zhou, F. Marsili, M. D. Shaw, V. B. Verma, S. W. Nam, D. Oblak, and W. Tittel, Phys. Rev. Lett. **119**, 083601 (2017).

[11] S.-l. Liu, Q. Zhou, Z.-y. Zhou, S.-k. Liu, Y. Li, Y.-h. Li, C. Yang, Z.-h. Xu, G.-c. Guo, and B.-s. Shi, Phys. Rev. A **100**, 013833 (2019).

[12] L. Chen, J. Lei, and J. Romero, Light: Sci. Appl. **3**, e153 (2014).

[13] Y. Zhang, D. England, A. Nomerotski, P. Svihra, S. Ferrante, P. Hockett, and B. Sussman, Phys. Rev. A **101**, 053808 (2020).

[14] S. Asban, K. E. Dorfman, and S. Mukamel, Proc. Natl. Acad. Sci. USA **116**, 11673 (2019).

[15] M. Erhard, M. Krenn, and A. Zeilinger, arXiv:1911.10006.

[16] A. Forbes and I. Nape, AVS Quantum Sci. **1**, 011701 (2019).

[17] A. Mair, A. Vaziri, G. Weihs, and A. Zeilinger, Nature **412**, 313 (2001).

[18] L. Neves, G. Lima, J. G. AguirreGomez, C. H. Monken, C. Saavedra, and S. Pádua, Phys. Rev. Lett. **94**, 100501 (2005).

[19] A. Vaziri, G. Weihs, and A. Zeilinger, Phys. Rev. Lett. **89**, 240401 (2002).

[20] G. Molina-Terriza, J. P. Torres, and L. Torner, Nat. Phys. **3**, 305 (2007).

[21] Y. Zhang, F. S. Roux, T. Konrad, M. Agnew, J. Leach, and A. Forbes, Sci. Adv. **2**, e1501165 (2016).

[22] S. P. Walborn, A. N. De Oliveira, R. S. Thebaldi, and C. H. Monken, Phys. Rev. A **69**, 023811 (2004).

[23] E. V. Kovlakov, I. B. Bobrov, S. S. Straupe, and S. P. Kulik, Phys. Rev. Lett. **118**, 030503 (2017).

[24] X.-M. Hu, J.-S. Chen, B.-H. Liu, Y. Guo, Y.-F. Huang, Z.-Q. Zhou, Y.-J. Han, C.-F. Li, and G.-C. Guo, Phys. Rev. Lett. **117**, 170403 (2016).

[25] M. Krenn, A. Hochrainer, M. Lahiri, and A. Zeilinger, Phys. Rev. Lett. **118**, 080401 (2017).

[26] J. Wang, S. Paesani, Y. Ding, R. Santagati, P. Skrzypczyk, A. Salavrakos, J. Tura, R. Augusiak, L. Mančinska, D. Bacco *et al.*, Science **360**, 285 (2018).

[27] M. Kues, C. Reimer, P. Roztocki, L. R. Cortés, S. Sciara, B. Wetzel, Y. Zhang, A. Cino, S. T. Chu, and B. E. Little, Nature **546**, 622 (2017).

[28] E. Bimbard, N. Jain, A. MacRae, and A. Lvovsky, Nat. Photon. **4**, 243 (2010).

[29] D. Grassani, S. Azzini, M. Liscidini, M. Galli, M. J. Strain, M. Sorel, J. Sipe, and D. Bajoni, Optica **2**, 88 (2015).

[30] Y.-H. Li, Z.-Y. Zhou, L.-T. Feng, W.-T. Fang, S.-l. Liu, S.-K. Liu, K. Wang, X.-F. Ren, D.-S. Ding, L.-X. Xu, and B.-S. Shi, Phys. Rev. Appl. **7**, 064005 (2017).

[31] M. Krenn, M. Huber, R. Fickler, R. Lapkiewicz, S. Ramelow, and A. Zeilinger, Proc. Natl. Acad. Sci. USA **111**, 6243 (2014).

[32] J. Torres, A. Alexandrescu, and L. Torner, Phys. Rev. A **68**, 050301(R) (2003).

[33] C. K. Law and J. H. Eberly, Phys. Rev. Lett. **92**, 127903 (2004).

[34] F. M. Miatto, A. M. Yao, and S. M. Barnett, Phys. Rev. A **83**, 033816 (2011).

[35] Y. Zhang and F. S. Roux, Phys. Rev. A **89**, 063802 (2014).

[36] A. M. Yao, New J. Phys. **13**, 053048 (2011).

[37] J. Romero, D. Giovannini, S. Franke-Arnold, S. M. Barnett, and M. J. Padgett, Phys. Rev. A **86**, 012334 (2012).

[38] H. Di Lorenzo Pires, H. C. B. Florijn, and M. P. Van Exter, Phys. Rev. Lett. **104**, 020505 (2010).

[39] J. P. Torres, A. Alexandrescu, S. Carrasco, and L. Torner, Opt. Lett. **29**, 376 (2004).

[40] L. Lu, P. Xu, M. Zhong, Y. Bai, and S. Zhu, Opt. Express **23**, 1203 (2015).

[41] Y.-L. Hua, Z.-Q. Zhou, X. Liu, T.-S. Yang, Z.-F. Li, P.-Y. Li, G. Chen, X.-Y. Xu, J.-S. Tang, J.-S. Xu *et al.*, Phys. Rev. A **97**, 013836 (2018).

[42] J. P. Torres, Y. Deyanova, L. Torner, and G. Molina-Terriza, Phys. Rev. A **67**, 052313 (2003).

[43] P. Machado, A. A. Matoso, M. R. Barros, L. Neves, and S. Pádua, Phys. Rev. A **99**, 063839 (2019).

[44] E. V. Kovlakov, S. S. Straupe, and S. P. Kulik, Phys. Rev. A **98**, 060301(R) (2018).

[45] S. Liu, Z. Zhou, S. Liu, Y. Li, Y. Li, C. Yang, Z. Xu, Z. Liu, G. Guo, and B. Shi, Phys. Rev. A **98**, 062316 (2018).

[46] S. Shi, M.-X. Dong, Y.-C. Yu, Y.-H. Ye, W. Zhang, K. Wang, G.-C. Guo, D.-S. Ding, and B.-S. Shi, Opt. Express **28**, 11538 (2020).

[47] Y. Zhang, F. S. Roux, M. McLaren, and A. Forbes, Phys. Rev. A **89**, 043820 (2014).

[48] Y. Zhang, M. Mclaren, F. S. Roux, and A. Forbes, Opt. Express **22**, 17039 (2014).

[49] L. Allen, M. W. Beijersbergen, R. J. C. Spreeuw, and J. P. Woerdman, Phys. Rev. A **45**, 8185 (1992).

[50] D. N. Klyshko, Sov. Phys. Uspekhi **31**, 74 (1988).

[51] R. T. Thew, K. Nemoto, A. G. White, and W. J. Munro, Phys. Rev. A **66**, 012303 (2002).

[52] D. Giovannini, J. Romero, J. Leach, A. Dudley, A. Forbes, and M. J. Padgett, Phys. Rev. Lett. **110**, 143601 (2013).

[53] A. Sanpera, D. Bruß, and M. Lewenstein, Phys. Rev. A **63**, 050301(R) (2001).

[54] J. Bavaresco, N. H. Valencia, C. Klöckl, M. Pivoluska, P. Erker, N. Friis, M. Malik, and M. Huber, Nat. Phys. **14**, 1032 (2018).

[55] N. Friis, G. Vitagliano, M. Malik, and M. Huber, Nat. Rev. Phys. **1**, 72 (2019).

[56] F. M. Dickey, *Laser Beam Shaping: Theory and Techniques* (CRC Press, Boca Raton, FL, 2018).

[57] C. Rosales-Guzmán and A. Forbes, *How to Shape Light with Spatial Light Modulators* (SPIE Press, Bellingham, WA, 2017).

[58] A. Laskin, N. Šiaulys, G. Šlekys, and V. Laskin, in *Laser Material Processing for Solar Energy Devices II*, Vol. 8826 (International Society for Optics and Photonics, Bellingham, WA, 2013), p. 88260F.

[59] S. Liu, C. Yang, Z. Xu, S. Liu, Y. Li, Y. Li, Z. Zhou, G. Guo, and B. Shi, Phys. Rev. A **101**, 012339 (2020).

[60] C. Brosseau, *Fundamentals of Polarized Light* (Wiley, New York, 1998).

[61] T. Durt, B.-G. Englert, I. Bengtsson, and K. Życzkowski, Int. J. Quantum Info. **8**, 535 (2010).

[62] M. Wieniak, T. Paterek, and A. Zeilinger, New J. Phys. **13**, 053047 (2011).

[63] E. Bolduc, N. Bent, E. Santamato, E. Karimi, and R. W. Boyd, Opt. Lett. **38**, 3546 (2013).

[64] S.-L. Liu, Q. Zhou, S.-K. Liu, Y. Li, Y.-H. Li, Z.-Y. Zhou, G.-C. Guo, and B.-S. Shi, Commun. Phys. **2**, 75 (2019).

[65] D. F. V. James, P. G. Kwiat, W. J. Munro, and A. G. White, Phys. Rev. A **64**, 052312 (2001).